

Strong C IV emission from star-forming galaxies: a case for high Lyman continuum photon escape

A. Saxena,¹  E. Cryer,¹ R. S. Ellis,¹ L. Pentericci,² A. Calabro,² S. Mascia,² A. Saldana-Lopez,³ D. Schaerer,^{3,4} H. Katz,⁵ M. Llerena⁶ and R. Amorín^{6,7}

¹Department of Physics and Astronomy, University College London, Gower Street, London WC1E 6BT, UK

²INAF – Osservatorio Astronomico di Roma, via Frascati 33, 00078, Monteporzio Catone, Italy

³Department of Astronomy, University of Geneva, 51 Chemin Pegasi, 1290 Versoix, Switzerland

⁴CNRS, IRAP, 14 avenue E. Belin, F-31400 Toulouse, France

⁵Astrophysics, University of Oxford, Denys Wilkinson Building, Keble Road, Oxford OX1 3RH, UK

⁶Departamento de Física y Astronomía, Universidad de La Serena, Av. Juan Cisternas 1200 Norte, La Serena, Chile

⁷Instituto de Investigación Multidisciplinaria en Ciencia y Tecnología, Universidad de La Serena, Raúl Bitrán, 1305 La Serena, Chile

Accepted XXX. Received YYY; in original form ZZZ

ABSTRACT

Finding reliable indicators of Lyman continuum (LyC) photon leakage from galaxies is essential in order to infer their escape fraction in the epoch of reionisation, where direct measurements of LyC flux are impossible. To this end, here we investigate whether strong C IV $\lambda\lambda 1548, 1550$ emission in the rest-frame UV spectra of galaxies traces conditions ripe for ample production and escape of LyC photons. We compile a sample of 19 star-forming galaxies in the redshift range $z = 3.1 – 4.6$ from the VANDELS survey that exhibit strong C IV emission, producing a stacked spectrum where all major rest-UV emission lines are clearly detected. Best-fitting spectral energy distribution models containing both stellar and nebular emission suggest the need for low stellar metallicities ($Z = 0.1 – 0.2 Z_{\odot}$), young stellar ages ($\log(\text{age}/\text{yr}) = 6.1 – 6.5$), a high ionisation parameter ($\log U = -2$) and little to no dust attenuation ($E(B - V) = 0.00 – 0.01$). However, these models are unable to fully reproduce the observed C IV and He II line strengths. We find that the Ly α line in the stacked spectrum is strong and peaks close to the systemic velocity, features that are indicative of significant LyC photon leakage along the line-of-sight. The covering fractions of low-ionisation interstellar absorption lines are also low implying LyC escape fraction in the range $\approx 0.05 – 0.30$, with signatures of outflowing gas. Finally, C IV/C III] ratios of > 0.75 for a subset of individual galaxies with reliable detections of both lines are also consistent with physical conditions that enable significant LyC leakage. Overall, we report that multiple spectroscopic indicators of LyC leakage are present in the stacked spectrum of strong C IV emitting galaxies, potentially making C IV an important tracer of LyC photon escape at $z > 6$.

Key words: galaxies: evolution – galaxies: high-redshift – dark ages, reionization, first stars – early Universe

1 INTRODUCTION

To understand the contribution of star-forming galaxies in governing cosmic reionisation, a process whereby the intergalactic medium (IGM) underwent a phase transition from a neutral to completely ionised gas, requires measures of their ionising photon production efficiencies, ξ_{ion} , the fraction of Lyman continuum (LyC; $\lambda_0 < 912 \text{ \AA}$) photons that manage to escape from the galaxy, f_{esc} (see [Dayal & Ferrara 2018](#), for a review) and the integrated space density of galaxies, derived from the UV luminosity functions (e.g. [Robertson et al. 2013, 2015; Bouwens et al. 2015; Finkelstein et al. 2015](#)).

The nature and strength of the ionising radiation emerging from young stars within star-forming galaxies can be derived from emission lines seen at rest-frame UV and optical wavelengths (e.g. [Gutkin et al. 2016; Feltre et al. 2016; Xiao et al. 2018; Plat et al. 2019](#)), including the Balmer line H α whose intensity is related to the number

of ionising photons produced through recombination physics (e.g. [Shivaei et al. 2018](#)). Detailed spectroscopic studies of galaxies at intermediate redshifts have provided reliable measurements of ξ_{ion} and we can expect continued progress within the reionisation era ($z \gtrsim 6$) following the successful deployment of the *James Webb Space Telescope (JWST)*.

Due to the increasing neutrality of the IGM at higher redshifts, however, direct measurements of LyC radiation from galaxies become challenging at $z \gtrsim 4$ (e.g. [Inoue et al. 2014](#)). A popular strategy for estimating f_{esc} for galaxies in the reionisation era is to study ‘analogues’ (i.e. with comparable physical properties) of $z > 6$ galaxies at intermediate redshifts ($z \sim 3$), for which LyC leakage can be directly observed (e.g. [Shapley et al. 2006](#)). With a detailed understanding of the nature of the stellar populations and conditions of the interstellar medium (ISM) in analogous intermediate redshift galaxies that exhibit high f_{esc} ([Nakajima et al. 2020; Saxena et al. 2022](#)), it may then be possible to infer which sources are likely to contribute most to driving cosmic reionisation.

* E-mail: aayush.saxena@ucl.ac.uk

However, although several dedicated searches have located LyC leaking galaxies from large area surveys at intermediate redshifts, their number remains quite modest (see [Meštrić et al. 2021](#), for a recent compilation). Inference from ground-based data, in particular, is restricted mostly to luminous galaxies (e.g. [Grazian et al. 2016](#); [Guaita et al. 2016](#); [Marchi et al. 2017](#); [Naidu et al. 2018](#); [Steidel et al. 2018](#); [Saxena et al. 2022](#)). A further complication in assessing the statistics of LyC leakers in any given survey is the expectation from numerical simulations that LyC leakage may be highly anisotropic, such that detections are only possible when the leaking channels are favourably aligned to the line-of-sight to the observer (e.g. [Katz et al. 2020](#); [Barrow et al. 2020](#); [Kimm et al. 2022](#)), with some observational evidence to support this idea (e.g. [Vanzella et al. 2021](#)).

Rather than undertaking a systematic survey for LyC leakage in a sample of photometrically-selected star forming galaxies, it may be more productive to study galaxies whose emission line properties are indicative of production of copious amounts of ionising photons with high ionisation parameters. Specific examples include sources with high $[\text{O III}]\lambda 5007/[\text{O II}]\lambda 3727$ ratios (e.g. [Nakajima et al. 2018a](#); [Izotov et al. 2018](#)), which may reflect density-bound nebulae from which LyC leakage may be possible ([Nakajima & Ouchi 2014](#)), as well as those with high ionisation energy lines which may reflect young stellar populations whose associated supernovae can clear channels that permit free passage of LyC photons ([Berg et al. 2019](#); [Nanayakkara et al. 2019](#); [Saxena et al. 2020b](#); [Tang et al. 2021](#); [Vanzella et al. 2021](#); [Senchyna et al. 2021](#)).

Following this strategy, in this paper we focus on consideration of the $\text{C IV}\lambda\lambda 1548, 1550$ doublet whose ionisation energy is 47.9 eV and which has already been detected in rest-UV spectra of several $z > 6$ galaxies (e.g. [Stark et al. 2015](#); [Mainali et al. 2017](#); [Schmidt et al. 2017](#), although it is not fully clear whether this C IV emission is only due to star-formation or due to active galactic nuclei or AGN). In the local universe, strong nebular C IV emission is almost exclusively seen in low-mass galaxies with extremely low metallicities ($\lesssim 0.1 Z_{\odot}$, where Z_{\odot} is the solar metallicity value), young stellar ages ($\log(\text{age}/\text{yr}) \lesssim 7$) and high specific star-formation rates ($\log(\text{sSFR}/\text{yr}^{-1}) < -8$; [Berg et al. 2016, 2018](#); [Senchyna et al. 2017, 2019](#)), properties that are likely common amongst galaxies in the reionisation era.

There is also growing evidence that strong C IV emission may be associated with LyC leakage: [Schaerer et al. \(2022\)](#) found strong C IV emission ubiquitously in a sample of $z < 0.7$ galaxies, and strong C IV has also been observed in a confirmed LyC leaker at $z \sim 3$ (e.g. [Vanzella et al. 2016](#)). [Schaerer et al. \(2022\)](#) interpreted their results with an elevated level of ξ_{ion} and the presence of density-bound H II regions. At low gas-phase metallicities, these conditions increase both the C IV luminosity as well as the $\text{C IV}/\text{C III}$ line ratio. Additionally, as a resonant line, C IV may trace photon escape through high-ionisation gas ([Berg et al. 2019](#)) and its typical P-Cygni profile is a valuable indicator of outflows driven by massive stars (e.g. [Steidel et al. 2016](#)) that are necessary to clear out channels for LyC escape. All the foregoing suggests C IV emission may be an important pointer to LyC leakage.

In this paper we investigate the properties of a sample of star-forming galaxies with spectroscopic redshifts at $z \sim 3.1-4.6$ selected purposely to exhibit strong C IV emission. Our aim is to better understand the spectroscopic properties of strong C IV emitting galaxies and, via independent spectroscopic measures, investigate the presence of signatures that may point towards significant LyC photon leakage. Our study complements ongoing efforts to understand the properties of star-forming galaxies that leak LyC photons at lower redshifts (e.g. Low-Redshift Lyman Continuum Survey, [Flury et al.](#)

[2022a,b](#) and the COS Legacy Archive Spectroscopy Survey, [Berg et al. 2022](#)). Ultimately, our study aims to provide a reference for an improved understanding and interpretation of *JWST*/NIRSpec spectra of star-forming galaxies at $z > 6$ in the context of LyC photon escape.

The layout of this paper is as follows. We describe the spectroscopic data, identification of C IV emitting galaxies, emission line measurements and flagging of potential AGN in §2. We present a stacked spectrum of C IV emitting galaxies along with a detailed analysis of other strong rest-frame UV emission lines in §3. We explore the nature of the underlying sources of ionisation that best describe the observed C IV emission (and other lines) in the stack in §4. Finally, we investigate whether significant LyC photon leakage can be inferred from the stacked spectrum of C IV emitting galaxies using other indirect spectral signatures in §5, summarising our findings in §6.

Throughout this paper, we assume a ΛCDM cosmology with $\Omega_m = 0.3$ and $H_0 = 67.7 \text{ km s}^{-1} \text{ Mpc}^{-1}$ taken from [Planck Collaboration et al. \(2016\)](#). All logarithms are in base 10, unless otherwise specified. In this paper we adopt a solar metallicity value of $Z_{\odot} = 0.02$.

2 DATA

We use spectroscopic data from VANDELS – a deep VIMOS survey of the CANDELS fields – which is a recently completed ESO public spectroscopic survey carried out using the VLT. VANDELS covers two well-studied extragalactic fields, the UKIDSS Ultra Deep Survey (UDS) and the Chandra Deep Field South (CDFS/GOODS-S). We refer the readers to [McLure et al. \(2018\)](#) for details about the survey description and target selection, and to [Pentericci et al. \(2018\)](#) for more information about data reduction and spectroscopic redshift determination. The final VANDELS data release, DR4¹, contains spectra of ~ 2100 galaxies in the redshift range $1.0 < z < 7.0$, with on-source integration times ranging from 20 to 80 hours, where $> 70\%$ of the targets have at least 40 hours of integration time ([Garilli et al. 2021](#)). The spectral resolution of VANDELS spectra is $R \sim 600$.

The reliability of redshifts in the VANDELS database is recorded using the following flags: 0 – no redshift could be assigned, 1 – 50% probability to be correct, 2 – 70-80% probability to be correct, 3 – 95-100% probability to be correct, 4 – 100% probability to be correct and 9 – spectrum shows a single emission line. The typical accuracy of spectroscopic redshift measurements is $\sim 150 \text{ km s}^{-1}$ ([Pentericci et al. 2018](#)).

2.1 A search for C IV emitters

In this work we only select spectroscopically confirmed galaxies from VANDELS that have a redshift reliability flag of either 3 or 4, which guarantees that the redshift measured by the VANDELS team has a $> 95\%$ probability of being correct. This also ensures reliable detection of multiple emission or absorption features in the spectrum.

Since our main goal is to explore spectroscopic properties of galaxies that show strong $\text{C IV}\lambda\lambda 1548, 1550$, we limit our focus to the redshift range $z = 3.1-4.6$ where additionally the $\text{Ly}\alpha$ line is visible in regions of high spectral throughput. We find 735 galaxies across the CDFS and UDS fields in the redshift range $z = 3.1-4.6$ and

¹ <http://vandels.inaf.it/dr4.html>

redshift reliability flags 3 or 4, which constitute the parent sample of this study.

We first visually inspect the 1D spectra of galaxies in the parent sample to search for signatures of C_{IV} emission. In cases where the C_{IV} line coincides with a skyline residual, we discard the source as any line flux measurement would be relatively unreliable. Once C_{IV} emission is identified in the 1D spectrum, we then inspect the 2D spectrum to ensure that the emission line in the 1D spectrum is real and not due to hot pixels, noise peaks and/or sky residuals.

Two of the co-authors independently performed the visual identification and only those that were sources identified as C_{IV} emitters by both individuals from 1D as well as 2D spectra are retained in our sample for further analysis. Out of 735 galaxies in the parent sample, we identify 22 sources as reliable C_{IV} emitters. None of these are detected in the deep *Chandra* X-ray catalogues in either CDFS (Luo et al. 2017) or in UDS (Kocevski et al. 2018) fields, ruling out any clear AGN activity.

We note here that the goal of this study is not to identify a complete sample of C_{IV} emitters in the VANDELS survey, but to explore the spectroscopic properties of sources that show clear evidence of strong C_{IV} emission at intermediate redshifts. Therefore, we do not include galaxies with marginal C_{IV} detections, or possible line emission that may be partly contaminated by a sky residual and would otherwise be considered as a real C_{IV} line. A more statistically complete sample of C_{IV} emitters from the VANDELS survey will be assembled in a future study (Mascia et al. in prep).

2.2 Rest-UV emission line measurements

We then measure all strong rest-frame UV emission lines visible in the spectra, which, in addition to C_{IV} mainly include Ly α , He II $\lambda 1640$ and O_{III} $\lambda\lambda 1660, 1666$. The line fitting is performed using the PYTHON package MPDAF², which provides tools to analyse spectra, images and data cubes, in a similar fashion to Saxena et al. (2020b). Briefly, we fit the observed emission lines with single Gaussian functions and measure the local continuum level in a wavelength range free of other emission lines on either side of the line.

From the fitted Gaussian we derive the line flux and full width at half maxima (FWHM), and use the local continuum level to measure the rest-frame equivalent widths (EW₀). Below we give a summary of the rest-frame UV lines identified in the individual spectra in this work.

By design, we identify C_{IV} emission in all 22 objects. The integrated line fluxes range from $0.2 - 6.0 \times 10^{-18}$ erg s⁻¹ cm⁻², with rest-frame equivalent widths ranging from EW₀ = 0.7 – 12.8 Å.

18 out of 22 objects show clear Ly α emission with a range of line strengths, widths and profiles. Three sources do not show any Ly α emission in their spectra and the Ly α line in one source is contaminated by a sky line.

Nine sources also show He II emission with signal-to-noise ratio (S/N) ≥ 2 , five of which were also identified by Saxena et al. (2020b) using an earlier data release of VANDELS. The integrated He II line fluxes range from $0.2 - 7.4 \times 10^{-18}$ erg s⁻¹ cm⁻² and EW₀ in the range 2.0 – 18.7 Å.

Nine sources show the O_{III} $\lambda\lambda 1660, 1666$ emission lines as well, which often appear to be blended and therefore only the total O_{III} flux is measured and reported. The O_{III} line fluxes range from $0.4 - 7.2 \times 10^{-18}$ erg s⁻¹ cm⁻², with EW₀ ranging from 1.5 – 11.3 Å.

² <https://mpdaf.readthedocs.io/en/latest/index.html>

The wavelength coverage of VANDELS spectra allows the detection of C_{III}] $\lambda 1909$ only at $z \lesssim 3.9$ in our sample. Additionally, since the C_{III}] line lies in a relatively red part of the observed spectrum it is more prone to contamination by skyline residuals. Therefore, we only robustly identify C_{III}] emission in 5 objects, with line fluxes ranging from $0.7 - 4.3 \times 10^{-18}$ erg s⁻¹ cm⁻², and EW₀ in the range 3.3 – 17.2 Å, which is comparable to a more statistical measurement of C_{III}] from VANDELS galaxies presented by Llerena et al. (2021).

The full suite of Ly α , C_{IV}, He II, and O_{III}] lines are detected with S/N ≥ 2 for only three sources in our sample, making it necessary to perform spectral stacking to boost S/N of other rest-UV emission lines that can enable characterising the properties of the underlying sources of ionising photons (see §3). However, before producing a stacked spectrum of C_{IV} emitters, we attempt to identify sources that may be dominated by AGN activity based on their C_{IV} and He II line strengths.

2.3 Identifying possible AGN

AGNs are capable of producing a much larger number of ionising photons through the accretion of material on to the central supermassive black hole, which results in a non-thermal spectral energy distribution that can easily produce extremely high energy photons giving rise to higher order transitions of the most common elements, such as C_{IV}, He II and N_V.

Since our sample is selected on the C_{IV} line and the second most common nebular emission line seen in individual galaxy spectra is He II, we use model predictions built around these two lines to identify possible AGN in our sample. In particular, we employ the diagnostic from Nakajima et al. (2018a), comparing the C_{IV}/He II ratio against EW₀(C_{IV}). The Nakajima et al. (2018a) emission line predictions are obtained using the photoionisation code Cloudy (Ferland et al. 2013). To model the spectral energy distribution (SED) of star-forming galaxies, the authors employ BPASS models (Stanway et al. 2016) that include the effect of interacting binary stars. The AGN models on the other hand assume a power law ionising radiation field emanating from the narrow-line region surrounding the active black hole.

In Figure 1 we show EW₀(C_{IV}) and C_{IV}/He II measured in the spectra of galaxies in our sample where both lines were detected with S/N > 2 . The dashed line demarcates the parameter space permitted by ionisation due to star-formation alone and ionisation due to AGN from Nakajima et al. (2018a). For comparison, we also show measurements from low metallicity dwarf galaxies in the local Universe (Berg et al. 2019; Senchyna et al. 2021), as well as C_{IV} measurements from a bright galaxy at $z \sim 7$ reported by Stark et al. (2015) and at $z \sim 6.1$ reported by Mainali et al. (2017).

We identify three sources in our sample that are likely to be dominated by AGN, whereas six sources occupy the parameter space where star-formation alone is enough to explain the C_{IV} and He II emission. For sources in our sample with no He II detection, the resulting lower limit on C_{IV}/He II is suggestive of ionisation due to star-formation. Since our goal is to investigate C_{IV} emission exclusively from star-forming galaxies, we remove these three potential AGN from our sample, leaving us with a final sample of 19 star-forming galaxies that show C_{IV} emission in their spectra.

We do note, however, that a few star-forming galaxies in our sample lie very close to the dividing line between photoionisation by AGN and star-formation. The parameter space occupied by our C_{IV} and He II emitting galaxies is comparable to the low mass, metal-poor galaxies in the nearby Universe that show high ionisation lines. We also note that the very strong C_{IV} detection in the $z \sim 7$ galaxy

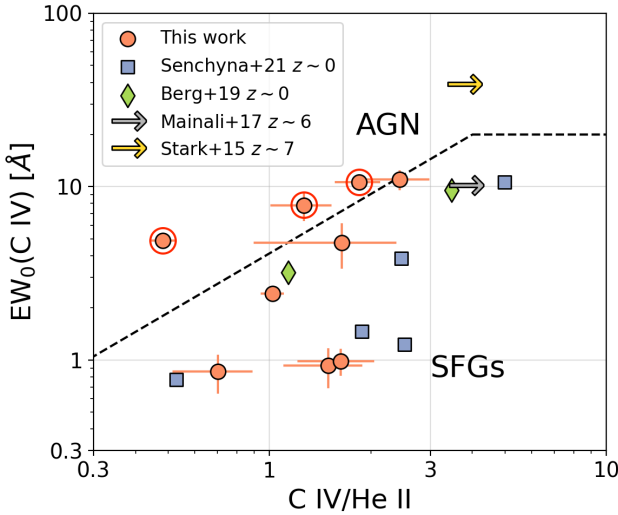


Figure 1. Distribution of C IV/He II flux ratio versus C IV rest-frame equivalent width for individual galaxies in this work where both emission lines are securely detected. The division between ionisation due to star-formation alone (SFG) and ionisation due to AGN has been adapted from the modelling of Nakajima et al. (2018a). Also shown for comparison are measurements from local low mass, low metallicity galaxies (Berg et al. 2019; Senchyna et al. 2021), as well as the C IV detection from a galaxy at $z \sim 7$ reported by Stark et al. (2015) and at $z \sim 6$ reported by Mainali et al. (2017). We find that three C IV emitters are likely to be dominated by AGN that are marked with red circles, and six galaxies can be explained through star-formation activity alone, lying close to the AGN-SFG dividing line implying the presence of sources hard ionising radiation. The three sources identified as AGN are removed from our final sample.

reported by Stark et al. (2015) suggests photoionisation due to AGN, however C IV measurement from the galaxy at $z \sim 6.1$ from Mainali et al. (2017) is comparable to what we find in our sample.

A histogram of the redshift distribution of 19 star-forming galaxies exhibiting strong C IV emission is shown in Figure 2. The median redshift of our sample is $z_{\text{med}} = 3.6$ and the sources span an observed *i*-band magnitude range of 24.4 – 26.7 AB.

3 A STACKED SPECTRUM OF C IV EMITTERS AT $3 < Z < 4.5$

As mentioned earlier, detecting the full suite of rest-UV emission (and absorption) features requires high S/N of the underlying continuum. Therefore, to boost S/N of these features to study the sample-averaged properties of C IV emitting galaxies and better understand their underlying stellar populations and state of the ISM, in this section we produce a stacked spectrum of galaxies in our final sample.

3.1 Stacking procedure

The method to co-add spectra adopted in this study is similar to Saxena et al. (2020b) – the stacking is performed by first de-redshifting each spectrum using the ‘systemic’ redshifts derived primarily from the strong C IV emission lines, as well as He II, O III] and C III] lines whenever visible in the individual galaxy spectrum. We generally find very good agreement with the systemic redshifts measured from these lines, which suggests that the C IV line in emission generally traces systemic redshifts well.

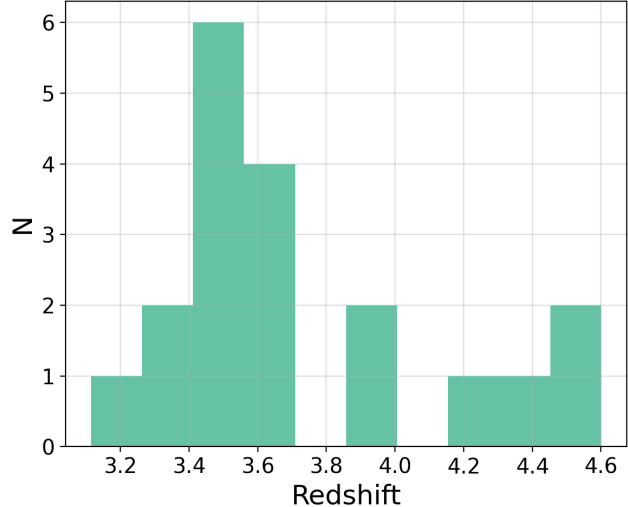


Figure 2. Redshift distribution of 19 C IV emitting star-forming galaxies in our final sample, selected from the VANDELS survey. The galaxies cover a redshift range of $3.1 < z < 4.6$, with a median redshift of $z = 3.6$.

The rest-frame spectra are normalised using the mean flux density value in the wavelength range 1460 – 1540 Å. Each spectrum is then assigned a weight based on the standard deviation of flux in this wavelength range, where the weight is inversely proportional to the measured variance on the flux density at ~ 1500 Å. The spectra are then re-sampled to a wavelength grid ranging from 1050 to 1820 Å, which is the rest-frame wavelength range most commonly probed by observed spectra in our sample, with a step size of 0.56 Å, which is the wavelength resolution obtained at a redshift of 3.6, the median redshift of our final sample.

The wavelengths in the observed individual spectra that do not fall within the rest-frame wavelength grid for the stacked spectrum are masked on a source by source basis to avoid incomplete sampling of the fluxes across galaxies. This means that the C III] line is unfortunately not covered in the stacked spectrum. We also mask residual sky lines and hot pixels in the spectra by employing a $> 20\sigma$ sigma-clipping. A stacked spectrum is then produced using a weighted averaging procedure, where as mentioned earlier the weights are the inverse of the variance in flux density at ~ 1500 Å.

The standard deviation of the stacked spectrum will have contributions both from S/N limitations of individual spectra as well as source-by-source spectral variation in the individual sources (e.g. Jones et al. 2012). Therefore, to capture both these effects, we use a bootstrapping method to calculate uncertainties on the stacked spectrum. To do this, we take our sample of 19 C IV emitters and replace one randomly selected C IV emitter by a C IV non-emitter selected from the parent VANDELS sample. We then produce a stacked spectrum of these 19 objects, with 18 C IV emitters and one non-emitter. We repeat this process of random replacement 500 times, consequently producing 500 stacked spectra with 18 C IV emitters and one non-emitter.

In this way, any strong spectral feature that is being contributed by an outlying C IV emitter can be accounted for, and the resulting standard deviation will be an accurate measure of the ‘true’ deviation of the stacked spectrum. The standard deviation of these bootstrapped spectra is used to calculate the 1σ uncertainty on the final stacked spectrum of C IV emitters. The final stacked spectrum along with 1σ errors is shown in Figure 3.

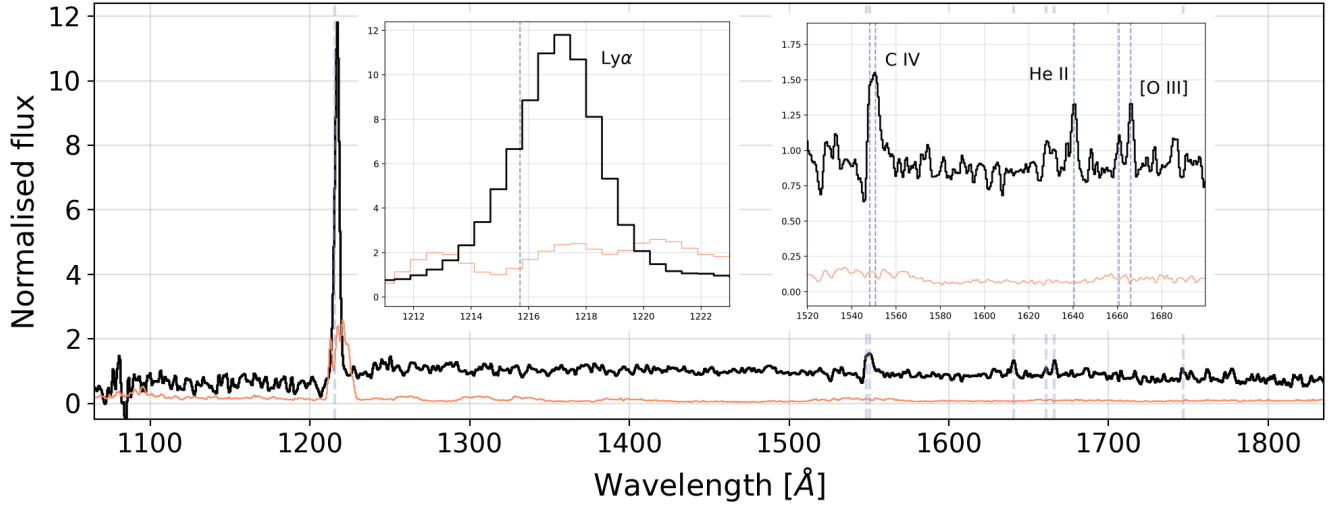


Figure 3. Stacked spectrum (black) of 19 C IV emitting star-forming galaxies in our final sample, with 1σ uncertainties (orange) obtained from bootstrapping. Multiple rest-frame UV emission lines are clearly detected in the stacked spectrum with high S/N. We show insets with the Ly α line (left), and C IV $\lambda\lambda 1548, 1550$, He II $\lambda 1640$ and O III] $\lambda\lambda 1660, 1666$ lines (right). We additionally mark the position of the N III] $\lambda 1747$ line in the spectrum, which is not as strong as the other lines highlighted. The equivalent widths and FWHMs of emission lines in the stacked spectrum are given in Table 1.

A range of emission and absorption features are clearly detected in the stacked spectrum, with the Ly α emission line appearing to be bright. In the sections that follow, we investigate the spectroscopic properties inferred from this stacked spectrum of C IV emitting galaxies, and below we briefly summarise and compare the observed properties of some of the brightest emission line features seen in the stack.

3.2 Emission lines

In this section we discuss the most prominent emission lines visible in the stacked spectrum. The emission lines are measured in a manner similar to that discussed in §2.2. The errors on both the line flux and width measurements are a consequence of the 1σ uncertainty on the stacked spectrum calculated via bootstrapping.

The Ly α line in the stack is strong and has a symmetric profile, with non-zero flux bluewards of the Ly α peak. The peak of the Ly α line is only slightly redshifted compared to the systemic redshift of the stacked spectrum. Such a line profile is typically associated with LyC emitting galaxies across redshifts (e.g. Verhamme et al. 2017; Gazagnes et al. 2020), which we investigate further in §5.1. A single Gaussian function provides a good fit to the line, with a measured FWHM of $820.0 \pm 17.0 \text{ km s}^{-1}$, and a high $\text{EW}_0 = 37.5 \pm 0.9 \text{ Å}$, placing it in the regime of strong Ly α emitting galaxies (LAEs).

Owing to the selection of our galaxy sample, we see strong C IV emission in the stacked spectrum. Due to the relatively low spectral resolution of the individual spectra, the two components at $\lambda 1548$ and $\lambda 1550$ are blended, requiring a double Gaussian function fit to recover the full line flux. From this fit we recover a total $\text{EW}_0(\text{C IV}) = 5.2 \pm 0.5$. A P-Cygni absorption feature immediately bluewards of the $\lambda 1548$ peak is also visible.

We further identify strong He II emission in the stacked spectrum. The emission line is fitted using a single Gaussian function, giving a $\text{FWHM}(\text{He II}) = 591.6 \pm 22.6 \text{ km s}^{-1}$, suggesting a nebular origin (e.g. Saxena et al. 2020b). The rest-frame equivalent width is $\text{EW}_0(\text{He II}) = 2.2 \pm 0.1 \text{ Å}$. With He $^+$ ionising potential being $\approx 54.4 \text{ eV}$, the presence of nebular He II emission in a galaxy spec-

Table 1. Properties of emission lines clearly detected in the stacked spectrum.

Line/Vacuum λ (Å)	EW_0 (Å)	FWHM (km s^{-1})
Ly α $\lambda 1216$	37.5 ± 0.7	830 ± 18
C IV $\lambda\lambda 1548, 1550$	5.2 ± 0.5	–
He II $\lambda 1640$	2.2 ± 0.1	592 ± 23
O III] $\lambda 1660$	1.1 ± 0.3	547 ± 34
O III] $\lambda 1666$	2.0 ± 0.1	502 ± 31
N III] $\lambda 1747$	1.2 ± 0.3	440 ± 120

Note. Since the C IV doublet appears to be blended and is fitted using a combination of two Gaussian functions, we do not report the FWHM.

trum is indicative of the presence of young stellar populations with low metallicities, capable of producing highly energetic photons.

We identify both O III] $\lambda\lambda 1660, 1666$ emission lines in the stacked spectrum, with the $\lambda 1660$ line being fainter than $\lambda 1666$. The doublet is sufficiently separated in wavelength such that two independent Gaussian functions can be fit to the lines. We measure a FWHM of $518.3 \pm 25.9 \text{ km s}^{-1}$ for $\lambda 1660$ and $611.0 \pm 30.8 \text{ km s}^{-1}$ for $\lambda 1666$. The total $\text{EW}_0(\text{O III})$ is $3.2 \pm 0.3 \text{ Å}$, with a O III] $\lambda 1660/\text{O III}] \lambda 1666$ ratio of ≈ 0.5 .

We also find N III] $\lambda\lambda 1747, 1749$ emission in the stacked spectrum, but the doublet appears to be blended. The N III] emission has a lower ionising potential of $\approx 26.9 \text{ eV}$, compared to O III] and other stronger lines visible in the stacked spectrum. The presence of N III] emission has not been widely reported – including from stacked spectra – in star-forming galaxies in the literature (but see Le Fèvre et al. 2019). However, the presence of N III] is not surprising considering that the sources were selected on emission lines requiring much higher ionising energies.

The EW_0 and FWHM of the above-mentioned lines are summarised in Table 1. In the following section we compare line measurements from our stacks to other stacked spectra of star-forming galaxies produced at comparable redshifts, as well as C IV emitting galaxies identified both in the local Universe as well as at $z > 6$.

3.3 Comparison with literature

The $\text{EW}_0(\text{Ly}\alpha)$ from our stack is comparable to that measured in the stacked spectrum of LBGs at $z \sim 3$ from [Steidel et al. \(2018\)](#) that were classified as LAEs ($\text{EW}_0(\text{Ly}\alpha) = 44.1 \text{ \AA}$), as well as the stacked spectrum of the quartile of their sources with the strongest Ly α emission, dubbed WQ4 ($\text{EW}_0(\text{Ly}\alpha) = 43.2 \text{ \AA}$). Both LAEs and WQ4 galaxies in [Steidel et al. \(2018\)](#) were identified to be the strongest LyC leakers using spectroscopic measurements. Interestingly, the strength of the C IV emission also appears to increase with increasing Ly α in the stacked spectra of [Steidel et al. \(2018\)](#), but no measure of C IV emission across stacks is given.

Comparing with the stacked spectra of narrow-band selected LAEs reported by [Nakajima et al. \(2018b\)](#), we find that our $\text{EW}_0(\text{Ly}\alpha)$ measurement is closest to that measured from the stacked spectrum of more UV-luminous LAEs having $\text{EW}_0(\text{Ly}\alpha) = 38 - 40 \text{ \AA}$. Prominent C IV features were also reported in their stacks of LAEs with large $\text{EW}_0(\text{Ly}\alpha)$ and fainter UV magnitudes, with $\text{EW}_0(\text{C IV})$ in the range $2.9 - 3.9 \text{ \AA}$. The $\text{EW}_0(\text{C IV})$ measured by [Nakajima et al. \(2018b\)](#) even for their strongest LAEs is lower than what we observe.

We then compare our measurements with the stacked spectra of LAEs at $3 < z < 4.6$ in the MUSE HUDF reported by [Feltre et al. \(2020\)](#). The C IV doublet in emission is seen in their stack of LAEs that have low FWHM(Ly α), high $\text{EW}_0(\text{Ly}\alpha)$ and faint UV magnitudes. The $\text{EW}_0(\text{C IV})$ ranged from $1.95 - 4.74 \text{ \AA}$. A slightly weaker He II emission with $\text{EW}_0(\text{He II}) \approx 1 - 1.3 \text{ \AA}$ was also reported from their stacks.

Only a handful of C IV observations currently exist at $z > 6$. The C IV emitter identified by [Stark et al. \(2015\)](#) at $z \sim 7$ shows a higher $\text{EW}_0(\text{Ly}\alpha) = 65 \pm 12 \text{ \AA}$ compared to our stack, a significantly higher $\text{EW}_0(\text{C IV}) \approx 40 \text{ \AA}$ with $\text{EW}_0(\text{He II}) < 11.4 \text{ \AA}$. However, there are suggestions that this source may be powered by an AGN, as we demonstrated in §2.3. The lensed C IV emitter at $z = 6.11$ from [Schmidt et al. \(2017\)](#) also has a higher $\text{EW}_0(\text{Ly}\alpha) = 68 \pm 6 \text{ \AA}$ and higher $\text{EW}_0(\text{C IV}) = 24 \pm 4 \text{ \AA}$ compared to our stack. Another lensed C IV emitter at $z \sim 6.1$ reported by [Mainali et al. \(2017\)](#) has a comparable $\text{EW}_0(\text{Ly}\alpha) = 40 \pm 5 \text{ \AA}$ with $\text{EW}_0(\text{C IV}) \approx 10$, which is higher than what is seen in our stack.

Two other highly magnified sources at $z = 4.77$ ([Matthee et al. 2022](#)) and at $z = 4.88$ ([Witstok et al. 2021](#)) show strong C IV, with $\text{EW}_0(\text{C IV}) \approx 5 \text{ \AA}$ and $\approx 18 \text{ \AA}$, respectively, which appear to be narrow and nebular in origin. These galaxies also show strong Ly α emission with $\text{EW}_0(\text{Ly}\alpha) \approx 62 \text{ \AA}$ and $\approx 143 \text{ \AA}$, respectively.

Turning our attention to comparable observations in the local Universe, [Senchyna et al. \(2019\)](#) and [Berg et al. \(2019\)](#) reported the detection of strong C IV emission with $\text{EW}_0(\text{C IV}) \approx 3 - 10 \text{ \AA}$ from two low-mass, metal-poor galaxies at $z \sim 0$ that also show strong He II emission. Strong and narrow He II emission has also been detected in these galaxies with $\text{EW}_0(\text{He II}) \approx 2.8$. Both studies concluded that stellar metallicities less than 10% solar (e.g. [Senchyna et al. 2021](#)) are required to explain this emission, and that these galaxies are likely analogues of reionisation era galaxies metal-poor star-forming galaxies.

Interestingly, rest-frame UV spectroscopy of LyC leakers at $z < 0.7$ has also resulted in the detection of strong C IV emission in all galaxies with $f_{\text{esc}} > 0.1$ ([Schaerer et al. 2022](#)), with some of the highest $\text{EW}_0(\text{C IV})$ seen in low- z star-forming galaxies. The $\text{EW}_0(\text{C IV})$ for a majority of their LyC leaking sources are comparable to that of our stacked spectrum.

Overall, the emission line features identified in the stacked spectrum of C IV emitters presented in this study appear to be consistent with those seen in strong LAEs at $z \sim 3 - 5$ and are somewhat rep-

resentative of the very limited detections of rest-UV emission from bright galaxies at $z > 6$. The line strengths in our sample also resemble those from extremely low-metallicity galaxies in the local Universe, as well as strong LyC leakers at $z \lesssim 1$.

4 UNDERLYING SOURCES OF IONISING PHOTONS

Having produced a stacked spectrum of strong C IV emitters and identified prominent rest-frame UV lines, in this section we compare the properties of the stacked spectrum with photoionisation models in a bid to constrain the dominant mechanism of ionising photon production within C IV emitting galaxies.

4.1 Spectral energy distribution (SED) fitting

We now find the best-fitting SED model for our stacked spectrum to understand the nature of ionising sources that could give rise to strong C IV emission (as well as other lines). We use models containing both continuum and nebular line emission produced by the BPASS team (e.g. [Xiao et al. 2018](#)). These models are built on stellar SEDs generated using BPASS v2.2.1 ([Stanway & Eldridge 2018](#)), which are then processed using the photoionisation code Cloudy, assuming a nebular gas cloud with density $\log(n_H / \text{cm}^{-3}) = 2.3$ and a spherical geometry to calculate nebular line fluxes³.

We consider stellar metallicities in the range $Z = 0.005 Z_{\odot}$ to $Z = 2 Z_{\odot}$, the stellar ages in the range $\log(\text{age/yr}) = 6 - 7.5$ and the dimensionless ionisation parameter, $\log(U)$ ⁴, in the range $[-1.0, -4.0]$. We additionally include a dust attenuation prescription derived by [Reddy et al. \(2016a\)](#) for $z \sim 3$ galaxies at rest-frame UV wavelengths, considering $E(B-V)$ values in the range $[0, 1]$ in steps of 0.01.

Since the Ly α line is prone to high levels of scatter, we focus our model comparison on the wavelength range $1300 - 1820 \text{ \AA}$ that contains C IV, He II and O III] lines. We then match the normalisation of the stacked spectrum and model SEDs using the *MinMaxScaler* tool that is part of the `PYTHON` package `SKLEARN`⁵, that scales features to lie between a minimum value of 0 and maximum value of 1.

To find the best-fitting SED to our stacked spectrum, we employ the root-mean-square deviation (RMSD) estimator. The RMSD estimator measures the differences between values predicted by a model and data, where the deviations represent the residuals. Low RMSD values indicate the closest agreement between models and data.

We populate a grid of models with varying combinations of metallicities, ages, ionisation parameters and dust attenuation in the ranges described above, calculating the RMSD for each model compared to the stacked spectrum. We find that two SEDs in particular give comparably good fits to the stacked spectrum, having the lowest RMSD values, which are described below and shown in Figure 4.

The first model (Model 1) has a stellar metallicity of $Z = 0.1 Z_{\odot}$, a stellar age of $\log(\text{age/yr}) = 6.5$, an ionisation parameter $\log(U) =$

³ <https://flexiblelearning.auckland.ac.nz/bpass/4.html>

⁴ SED models often tend to employ the dimensionless ionisation parameter, U , which gives the ratio of the density of ionising photons to the density of hydrogen. The ionising photon production efficiency or ξ_{ion} , on the other hand is the number of ionising photons produced per unit UV luminosity. Under assumptions of hydrogen density for a given UV luminosity, U and ξ_{ion} are closely related to one another and broadly trace the ionising photon production capabilities of a source.

⁵ <https://scikit-learn.org/stable/modules/generated/sklearn.preprocessing.MinMaxScaler.html>

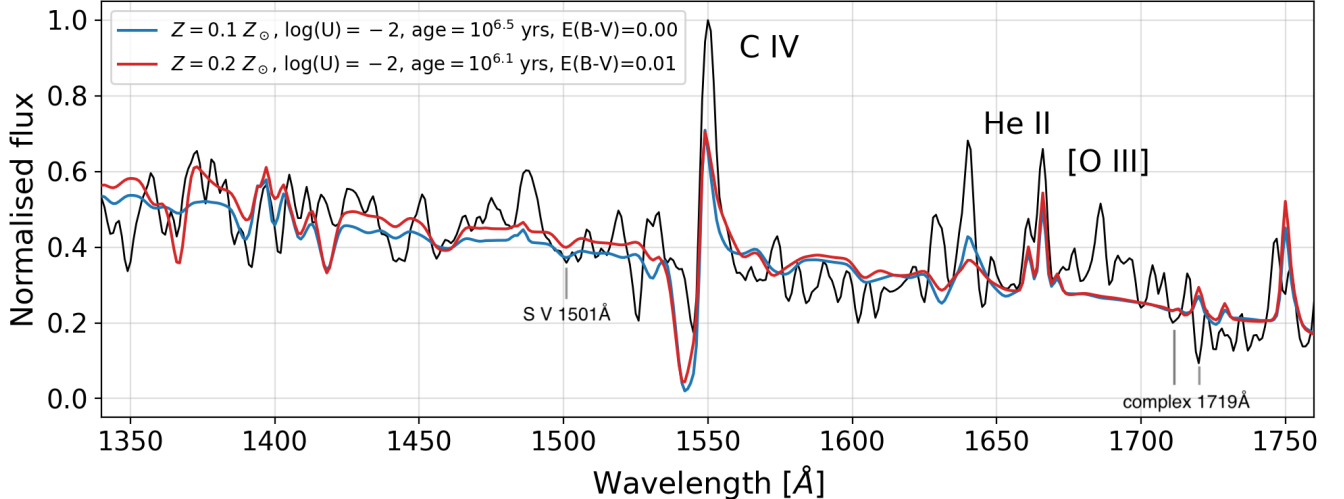


Figure 4. Zoom-in of the wavelength range covering C IV, He II and O III] emission lines in the stacked spectrum of C IV emitters. The spectrum has been normalised using minimum-maximum scaling to aid comparisons with SED models, which have also been smoothed to the VANDELS spectral resolution. We show the two best-fitting spectral energy distribution (SED) models. Model 1 (blue) has a stellar metallicity of $Z = 0.1 Z_{\odot}$, $\log(\text{age/yr}) = 6.5$, an ionisation parameter of $\log(U) = -2.0$ and no dust attenuation. Model 2 (red) has a higher stellar metallicity of $Z = 0.2 Z_{\odot}$, a lower stellar age of $\log(\text{age/yr}) = 6.1$, an ionisation parameter of $\log(U) = -2.0$ and a small dust attenuation of $E(B - V) = 0.01$. We find that both models are able to reproduce the P-Cygni profile of C IV, but under-predict the C IV and He II lines. The models match the O III] doublet strength as well as their ratio reasonably well. Overall, the best-fitting SED models suggest that young and low-metallicity starbursts with a high ionisation parameter are needed to explain the observed C IV (and He II) in the stacked spectrum. We additionally mark the locations of the absorption features used to independently measure stellar metallicities in §4.2: S V at 1501 Å and a blend of N IV, Si IV, Al II and Fe IV at 1719 Å. Finally, we note that the emission feature at 1486.5 Å is from N IV] and the feature spotted near ≈ 1680 Å is likely a noise fluctuation.

Table 2. Properties of the best-fitting BPASS+Cloudy SED models

	Z/Z_{\odot}	$\log(\text{age/yr})$	$\log(U)$	$E(B - V)$	RMSD
Model 1	0.1	6.5	-2.0	0.00	0.098
Model 2	0.2	6.1	-2.0	0.01	0.099

-2.0 with no dust attenuation, $E(B - V) = 0.0$, shown in blue in Figure 4. Model 1 reproduces the C IV emission line's P-Cygni profile but under-predicts the line flux. The model produces He II emission, but not enough to match the observed line emission. Model 1 is able to reproduce the O III] doublet line strengths and ratios, as well as N III] emission, also matching the observed UV slope of the stacked spectrum.

The second model (Model 2) has a higher stellar metallicity of $Z = 0.2 Z_{\odot}$ compared to Model 1, with a lower stellar age of $\log(\text{age/yr}) = 6.1$, $\log(U) = -2.0$ and a small dust attenuation of $E(B - V) = 0.01$, shown in red in Figure 4. This model is also able to reproduce the C IV line profile but under-predicts its line flux. Model 2 produces weaker He II emission in comparison to Model 1, but is able to reproduce the O III] and N III] emission. Model 2 also matches the observed UV slope in the spectrum. Both Models 1 and 2 have highly comparable RMSD values, and their properties are summarised in Table 2.

Both well-fitting SEDs imply that stellar populations with metallicities of $0.1 - 0.2 Z_{\odot}$, low stellar ages and relatively high ionisation parameters are needed to reproduce the vast majority of the observed rest-UV emission lines and match the UV slope of the stacked spectrum of C IV emitting sources. Interestingly, the largest discrepancy between observations and model predictions are for emission lines requiring higher ionisation energies. For example, the O III] and N III] lines that require energies of 35.1 eV and 29.6 eV, respectively, are

relatively well produced by both models, but the C IV and He II lines requiring energies of 47.9 eV and 54.4 eV are under-predicted.

This suggests that the best-fitting SEDs are unable to produce ionising radiation fields that are 'hard' enough, such that a large amount of photons with extremely high energies are produced, which we discuss further in §4.3. We note here that increasing the ionisation parameter of these models results in a catastrophic mismatch between the observed and predicted UV slopes, which is not significantly improved by increased dust attenuation, leading to sub-optimal fits.

4.2 Stellar metallicity from absorption indices

In addition to inferring the stellar metallicities from SED fitting, we also measure the stellar metallicity of the stacked spectrum in a more direct manner using rest-frame UV absorption lines.

We note the presence of absorption features due to ionised S V at ≈ 1501 Å and due to a blend of N IV, Si IV, Al II and Fe IV at ≈ 1719 Å. These features arise as a result of absorption in the stellar photospheres of young, hot stars, and the strength of absorption can be used as a reliable tracer of stellar metallicity, independent of age of the stars or their initial mass function (e.g. Calabro et al. 2021, and references therein).

We measure $\text{EW}_0(1501) = -1.0 \pm 0.5$ Å and $\text{EW}_0(1719) = -1.3 \pm 1.0$ Å and using the metallicity calibrations from Calabro et al. (2021) that use BPASS models without any nebular emission, we obtain a stellar metallicity of $Z = 0.0036 \pm 0.0025$ from the 1501 index and a comparable $Z = 0.0041 \pm 0.0031$ from the 1719 index. Using the solar metallicity value of $Z_{\odot} = 0.02$ as before, both these independent metallicity measurements suggest stellar metallicities of $Z \approx 0.2 Z_{\odot}$, agreeing within the uncertainties.

These independent metallicity measurements are consistent with Model 2 presented in §4.1, suggesting that galaxies exhibiting strong

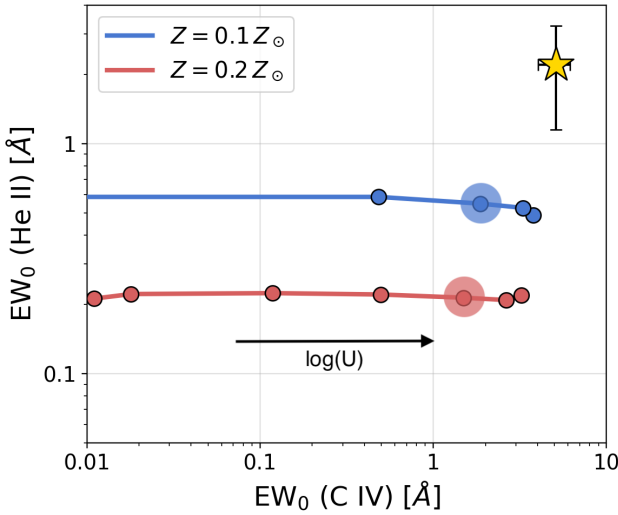


Figure 5. Comparison of the $EW_0(\text{C IV})$ and $EW_0(\text{He II})$ measured in the stacked spectrum (gold star) with predictions from best-fitting models: Model 1 with $Z = 0.1 Z_\odot$, $\log(\text{age/yr}) = 6.5$ (blue) and Model 2: $Z = 0.2 Z_\odot$, $\log(\text{age/yr}) = 6.1$ (red). The best-fitting ionisation parameter values of $\log(U) = -2$ for both models are highlighted. Particularly for Model 2, which has a consistent metallicity with that inferred from absorption features, the He II line strength is under-predicted by an order of magnitude and the C IV line strength by a factor of ~ 3 . Additional sources of high-energy ionising photons may be needed to explain the observed emission line strengths.

C IV requiring high ionising photon energies do not necessarily have abnormally low metallicities. For example, measurements from galaxies in the VANDELS survey at $z \sim 3.5$ suggest average stellar metallicities in the range $Z \approx 0.1 - 0.2 Z_\odot$ (Cullen et al. 2020; Calabro et al. 2021), as inferred both from absorption indices as well as best-fitting SED models. For comparison, known C IV and He II emitters in the local Universe almost always have extremely low stellar (and gas phase) metallicities of the order $Z \lesssim 0.1 Z_\odot$ (e.g. Berg et al. 2019; Senchyna et al. 2021).

4.3 Under-prediction of C IV and He II

We note again that neither of the two best-fitting SEDs presented in §4.1 is able to fully reproduce the observed C IV and/or He II emission in the stacked spectrum. This is also shown clearly in Figure 5, where the ionisation parameter increases from right to left, with the highest value $\log(U) = -1.0$. The best-fitting $\log(U)$ value of -2 obtained from SED fitting has been highlighted for both models.

Looking at Model 2 with $Z = 0.2 Z_\odot$ that is consistent with the independent metallicity measurements from absorption indices, the He II EW_0 is under-predicted by an order of magnitude at $\gtrsim 3\sigma$ significance, whereas the C IV line is under-predicted by a factor of ~ 3 , also with $\gtrsim 3\sigma$. The discrepancy between observed and predicted equivalent widths also exists when comparing with Model 1, but Model 1 produces stronger He II in comparison to Model 2, bringing the tension down to $\sim 2\sigma$. The discrepancy with the C IV line, however, remains at $\sim 3\sigma$.

An under-predicted He II equivalent width even by the lowest metallicity models from BPASS was previously also reported by Saxena et al. (2020b). To account for the ‘missing’ He II ionising photons within such galaxies, Saxena et al. (2020b) suggested the inclusion of additional sources of ionisation such as faint AGN, stripped binary stars (e.g. Götzberg et al. 2019) or ultra-luminous X-ray sources (e.g.

Schaerer et al. 2019; Saxena et al. 2020a; Simmonds et al. 2021; Umeda et al. 2022).

One additional scenario that may explain strong C IV and He II emission is a recent starburst event (preferentially from metal-poor gas) within galaxies that harbour relatively enriched ($Z \gtrsim 0.2 Z_\odot$) stellar populations. Evidence for the presence of both young and evolved stellar populations in high-redshift galaxies that show strong emission lines has already been recently discussed: broadband SED fitting and Atacama Large Millimetre Array (ALMA) observations of hyperfine transition metal lines of galaxies at $z \gtrsim 9$ have suggested that these may already harbour evolved stellar populations (e.g. Roberts-Borsani et al. 2020; Laporte et al. 2021). Recently, Tang et al. (2022) also reported the presence of evolved stellar populations in extreme [O III] $\lambda 5007$ emitting galaxies at redshifts 1.3–3.7, where this evolved population can be up to ~ 40 times more massive than the young starburst associated with the extreme line emission.

Therefore, galaxies undergoing periods of starburst activity may temporarily be able to produce copious amounts of high-energy photons (i.e., periods of high ξ_{ion}), giving rise to strong emission lines such as C IV, and He II, as well as [O III] $\lambda 5007$. Radiative transfer calculations in zoom-in simulations of galaxy formation from Barrow et al. (2020) showed that periods of high ξ_{ion} are often coincident with periods of extreme emission line strengths driven by starburst events. Periods of high LyC f_{esc} tend to then follow, once the gas has been blown out and channels of low absorption have been established over a timescale of \sim Myrs due to rampant supernova activity. Having seen evidence of elevated ionising photon production in C IV emitting galaxies, in the next section we investigate whether C IV emitters may also trace conditions that enable a higher fraction of LyC photons to escape into the IGM.

5 C IV EMITTERS AS TRACERS OF HIGH IONISING PHOTON ESCAPE

The primary goal of this paper is to investigate whether C IV emitting galaxies at intermediate redshifts trace conditions that might enable a high LyC f_{esc} , which we test in this section using indirect indicators in rest-UV in the stacked spectrum.

5.1 Inference from Ly α strength and velocity offset

Useful information regarding the presence of channels in the ISM, allowing for a high escape fraction of LyC photons, can be obtained from both the strength (e.g. Dijkstra 2014), the profile and the velocity offset of the Ly α emission line (e.g. Verhamme et al. 2015). The redshift range of our targets ensures that the Ly α line is visible for all galaxies, and in this section we use the observed Ly α emission in the stacked spectrum to explore the possibility of high LyC f_{esc} from C IV emitting galaxies.

It has been shown that galaxies with high LyC f_{esc} often have the peak of the Ly α emission line close to the systemic redshift, with non-zero Ly α flux bluewards of the systemic redshift (Verhamme et al. 2015; Dijkstra et al. 2016). In this scenario, both Ly α and LyC photons would be able to escape the H II regions within which they are produced with relative ease through a porous ISM. This has also been verified observationally through Ly α profiles of low redshift LyC leakers, with an anti-correlation observed between LyC f_{esc} and the separation of the Ly α blue and red peaks as well as velocity offset from systemic (e.g. Izotov et al. 2018, 2021).

We find that the velocity offset of the Ly α line in the stacked spectrum compared to the systemic redshift is relatively small at

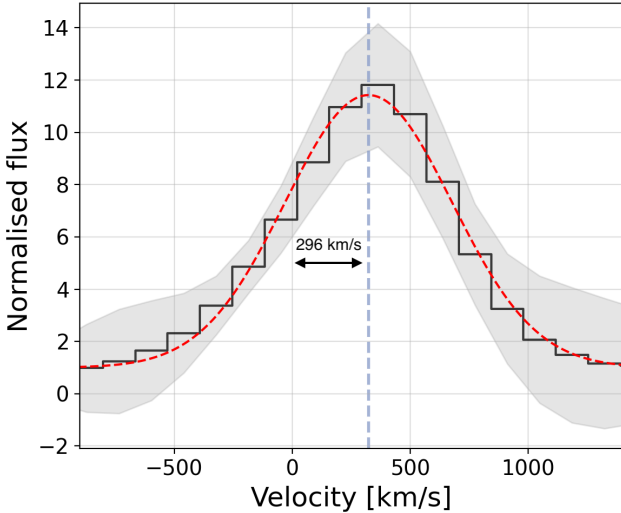


Figure 6. Zoom-in of the Ly α emission line in the stacked spectrum in units of velocity, with $v = 0$ tracing the systemic velocity constrained using the C IV $\lambda 1550$ feature in the stack. The velocity offset of the Ly α peak is $\approx 300 \text{ km s}^{-1}$ compared to the systemic velocity and there is significant flux bluewards of the Ly α peak. The line profile is highly symmetric. All of these Ly α features are consistent with expectations from galaxies that may or do indeed show a high escape fraction of LyC photons (e.g. Verhamme et al. 2015, 2017).

$v \approx 296 \pm 20 \text{ km s}^{-1}$, as shown in Fig 6. We also note that the Ly α emission is strong and appears to be symmetric with non-zero flux bluewards of the Ly α peak, although this could also be a consequence of stacking objects with a variety of line profiles, resulting in an overall Gaussian distribution. The strength and the low velocity offset compared to systemic, however, are consistent with predictions from Verhamme et al. (2015) of high Ly α and LyC escape.

To put the observed Ly α strength and velocity offset observed in the stacked spectrum of C IV emitters in the global context of star-forming galaxies at $z \sim 3.6$, we compare our measurements to stacked spectra of 19 randomly selected star-forming galaxies from the VANDELS parent sample with the same range of UV luminosities and redshifts, and redshift quality flags as the C IV emitters. We repeat the stacking process 500 times following the methodology outlined in §3, obtaining a distribution of stacked spectra of non-C IV emitters randomly drawn from VANDELS. We then measure the strength of Ly α emission in each stack as well as the offset of the peak of Ly α emission from the expected ‘systemic’ redshift, using the spectroscopic redshifts compiled by the VANDELS team as reference.

We show the results of this exercise in Fig 7, where it is clear that the stack of C IV emitters not only shows a $\text{EW}_0(\text{Ly}\alpha)$ value that is 5σ higher than the median Ly α EW measured from randomly stacking VANDELS spectra, its velocity offset compared to the systemic redshift is also 3σ lower than the median offset. We also generally find that stronger Ly α lines tend to peak closer to the systemic redshift, which has also been observed in the literature (see Erb et al. 2014, for example).

Also shown in Figure 7 are Ly α measurements from LyC leakers identified by Fletcher et al. (2019) from a sample of narrow-band selected LAEs, which all exhibit comparable Ly α line strengths and offsets from the systemic velocity to that seen in our stacked spec-

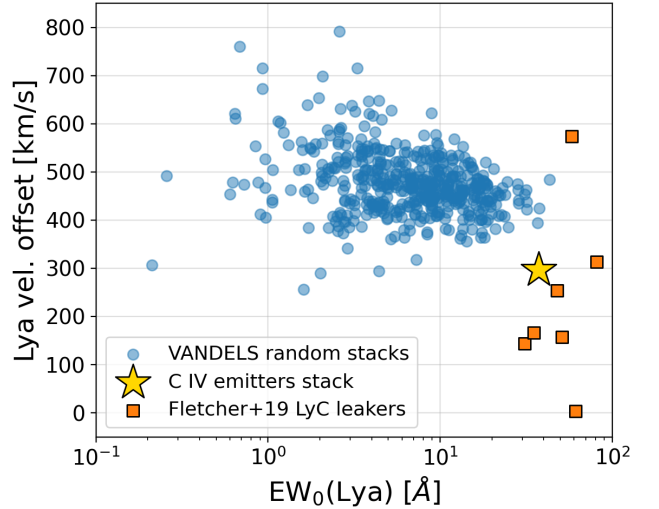


Figure 7. Distribution of Ly α EW_0 and velocity offset from systemic redshift measured from the stacked spectrum of C IV emitters, compared with measurements from 500 iterations of stacking 19 randomly drawn galaxies from the VANDELS survey occupying the same redshift range as the C IV emitters. The Ly α strength and velocity offset of C IV emitters is an outlier compared to the distribution inferred from randomly selected VANDELS galaxies, implying that the Ly α emission line from C IV emitting galaxies is indicative of high LyC f_{esc} (e.g. Verhamme et al. 2015). We additionally show Ly α measurements from LyC leakers at $z \sim 3$ presented in Fletcher et al. (2019), which also exhibit strong Ly α as well as low velocity offset from the systemic redshift.

trum⁶. This suggests that galaxies with strong C IV emission in their spectra preferentially show stronger Ly α emission that peaks close to the systemic redshift, which is often seen in the spectra of LyC leaking galaxies across redshifts.

Other known LyC leaking galaxies at high redshifts in the literature show similar Ly α strengths and profiles, with Ly α from the *Sunburst Arc* at $z = 2.4$ (Rivera-Thorsen et al. 2019), *Ion2* at $z = 3.2$ (Vanzella et al. 2016) and *Ion3* at $z = 4.0$ (Vanzella et al. 2018) peaking close to systemic $v = 0$ with non-zero flux bluewards of the peak. High resolution spectra for such galaxies have revealed multiple peak Ly α morphologies, indicative of ionising photon escape channels in the neutral H I gas (e.g. Vanzella et al. 2018).

The Ly α line seen in our stacked spectrum is also comparable to that of the stacked spectrum of the subsets of LAEs at $z \sim 2$ that are likely leaking significant LyC radiation presented by Naidu et al. (2022). Those authors also find C IV emission in the stacked spectrum of candidate LyC leakers, with no C IV emission detected in the stack of LAEs that are unlikely to be leaking LyC photons.

Due to the relatively low spectral resolution of our stacked spectrum we are unable to resolve the Ly α line, however future higher resolution observations of the Ly α line profile of C IV emitting galaxies would be valuable to further investigate the presence of Ly α /LyC escape channels.

⁶ Here we use all candidate LyC leaking galaxies in the Fletcher et al. (2019) sample that have robust $\text{EW}_0(\text{Ly}\alpha)$ measurements from spectroscopy, with additional accurate determination of their systemic redshifts from other lines. These galaxies belong to both the *Gold* (4 galaxies) and *Silver* (3 galaxies) sub-samples.

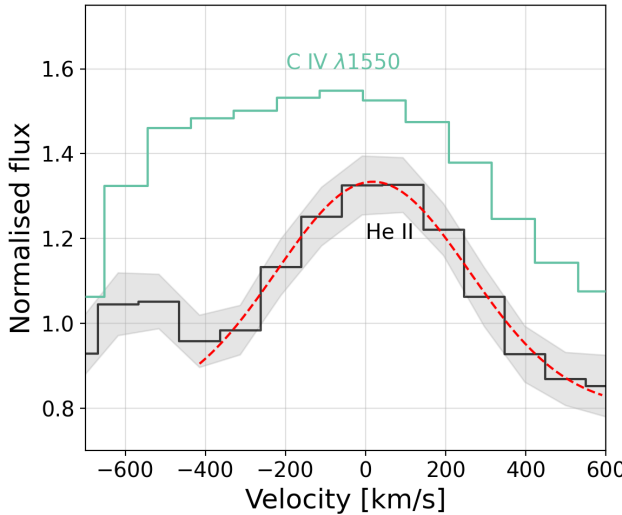


Figure 8. Velocity profile of He II emission (black) in the stacked spectrum shown alongside the C IV emission (green), with $v = 0$ tracing the systemic velocity. The He II line is well-fit with a single Gaussian (red dashed line) with the peak of the Gaussian within $\approx 50 \text{ km s}^{-1}$ of the systemic velocity. The presence of both C IV and He II emission lines requires the production of extremely high-energy photons ($E > 47.9$ and $E > 54.4 \text{ eV}$ for C IV and He II, respectively). We find a relatively high He II/C IV ratio of ≈ 0.5 , which is indicative of extremely high ionising photon production efficiencies of $\log(\xi_{\text{ion}}) \gtrsim 25.6 \text{ erg}^{-1} \text{ Hz}$ (e.g. [Berg et al. 2019](#); [Schaerer et al. 2022](#)).

5.2 Presence of strong He II

We also find strong He II emission in addition to C IV emission in the stacked spectrum, with $\text{He II/C IV} \approx 0.5$, indicative of the presence of sources capable of producing hard ionising radiation fields (see also [Berg et al. 2018, 2019](#)). [Schaerer et al. \(2022\)](#) also showed the presence of He II emission in strong LyC leaking galaxies at $z < 0.7$, with high equivalent widths of $3 - 8 \text{ \AA}$, which can be explained with relatively high ionising photon production efficiencies, $\log(\xi_{\text{ion}}) \approx 25.6 - 25.8 \text{ erg}^{-1} \text{ Hz}$. These line strengths are higher than $\text{EW}_0(\text{He II}) = 2.6$ that we measure from our stacked spectrum, but the relatively high He II/C IV ratio we find is comparable to that seen in the spectra of LyC leakers presented by [Schaerer et al. \(2022\)](#), indicative of similarly high ξ_{ion} .

In Figure 8 we show the velocity profile of the observed He II emission with respect to the C IV line, finding that the peak of He II emission is within $\approx 50 \text{ km s}^{-1}$ to that of C IV, which is indicative of the alignment of channels through which photons with much higher energies may escape as well, in addition to the relatively lower energy channels traced by Ly α . With C IV being a resonant line, the peaks of C IV and He II being coincident suggests that the resonant scattering does not dramatically alter the energies of escaping photons, pointing towards the presence of well-defined columns in the multi-phase ISM facilitating high-energy ionising (and possibly LyC) photon escape.

Further, [Naidu et al. \(2022\)](#) also found He II emission in the stacked spectra of candidate LyC leaking LAEs at $z \sim 2$ with $\text{EW}_0(\text{He II}) \approx 2 \text{ \AA}$, which is highly comparable to our measurement. However, [Marques-Chaves et al. \(2022\)](#) reported the detection of comparable He II $\lambda 4686$ emission from LyC leakers and non-leakers $z \sim 0.2 - 0.4$, noting that metallicity and not LyC escape is the dominant factor in setting He II line strengths. Their study implies that LyC leaking galaxies may not show systematically ‘harder’ ionising spectra compared to non-leakers at similar metallicities, casting doubt on the

presence of He II emission as a standalone indicator of strong LyC leakage. Nonetheless, strong He II emission in our stacked spectrum of C IV emitters, when combined with other indicators, may still favour high f_{esc} .

5.3 Insights from low-ionisation interstellar absorption

In this section we attempt to infer LyC f_{esc} from both the depths and the profiles of absorption features in the stacked spectrum of C IV emitters arising from singly ionised species in the ISM. A low covering fraction ($f_c < 1$) of metal-enriched gas, and consequently of that of H I gas, is expected to be a necessary but not sufficient condition for significant LyC photon escape, and several studies have investigated this relationship using rest-UV absorption lines ([Jones et al. 2013](#); [Henry et al. 2015](#); [Reddy et al. 2016b](#); [Leethochawalit et al. 2016](#); [Reddy et al. 2022](#); [Steidel et al. 2018](#); [Chisholm et al. 2018](#); [Saldana-Lopez et al. 2022](#)).

Since the wavelength range of our stacked spectrum does not cover the H I Lyman-series transitions of Ly β and beyond, we focus instead on two other well-studied low-ionisation interstellar (LIS) absorption features at rest-UV wavelengths, C II $\lambda 1334$ and Si II $\lambda 1260$ and $\lambda 1526$. We do not use the Si II $\lambda 1304$ feature as it appears to be contaminated by O I $\lambda 1302$.

Following [Jones et al. \(2013\)](#), we calculate the covering fraction of the above mentioned transitions assuming a ‘picket fence’ like distribution of optically thick gas clouds and optically thin ‘holes’ in the ISM (e.g. [Steidel et al. 2018](#)). Within the gas clouds, the column density of gas is assumed to be high enough such that it appears optically thick ($\tau \gg 1$) at the absorbing wavelength, saturating the absorption lines. In this picture, the covering fraction may be calculated as $f_c = 1 - I(\lambda)/I_0$, where I_0 is the local continuum level and $I(\lambda)$ is the residual intensity in the spectrum (see also [Saldana-Lopez et al. 2022](#)).

We measure $\text{EW}_0(\text{LIS})$ following the methodology of [Saldana-Lopez et al. \(2022\)](#) by first locating the minimum depth of the absorption line in question and then integrating over a velocity range of $\pm 1250 \text{ km s}^{-1}$, dividing the measured flux by the model stellar continuum. Since we use the convention whereby emission lines have positive equivalent widths, the equivalent width measured for absorption features in this work are negative. We find $\text{EW}_0(\text{Si II } \lambda 1260) = -0.61 \text{ \AA}$, $\text{EW}_0(\text{Si II } \lambda 1526) = -0.80 \text{ \AA}$ and $\text{EW}_0(\text{C II } \lambda 1334) = -0.69 \text{ \AA}$. These LIS absorption features along with strong Ly α and C IV lines are shown in Figure 9. Once again, $v = 0$ is set to be at the peak of the C IV $\lambda 1550$ emission. The shaded regions show 1σ uncertainties calculated using bootstrapping in §3. We note that both emission and absorption features have been continuum normalised, and the Ly α emission has been re-scaled to aid visualisation.

Inferring limits on f_{esc} directly from the covering fraction of LIS lines (e.g. [Jones et al. 2013](#)), we can place limits of $f_{\text{esc}} < 0.8$ from the stacked spectrum of C IV emitters. Using the the average $\text{EW}_0(\text{LIS}) \approx -0.70 \pm 0.8 \text{ \AA}$ and the relation between f_{esc} and $\text{EW}_0(\text{LIS})$ obtained by [Saldana-Lopez et al. \(2022\)](#), the f_{esc} is estimated to be in the range $\sim 0.05 - 0.30$. Finally, from only $\text{EW}_0(\text{C II } \lambda 1334)$ using the [Mauerhofer et al. \(2021\)](#) relation we infer $f_{\text{esc}} > 0.1$. All of these estimates point towards significant f_{esc} from galaxies that show strong C IV emission in their spectra.

We further note that the peaks of the absorption features are blue-shifted with respect to the systemic velocity, indicative of the presence of outflowing gas (e.g. [Jones et al. 2013](#)). We infer outflow velocities in the range $-500 \lesssim v \lesssim -200 \text{ km s}^{-1}$, which are within

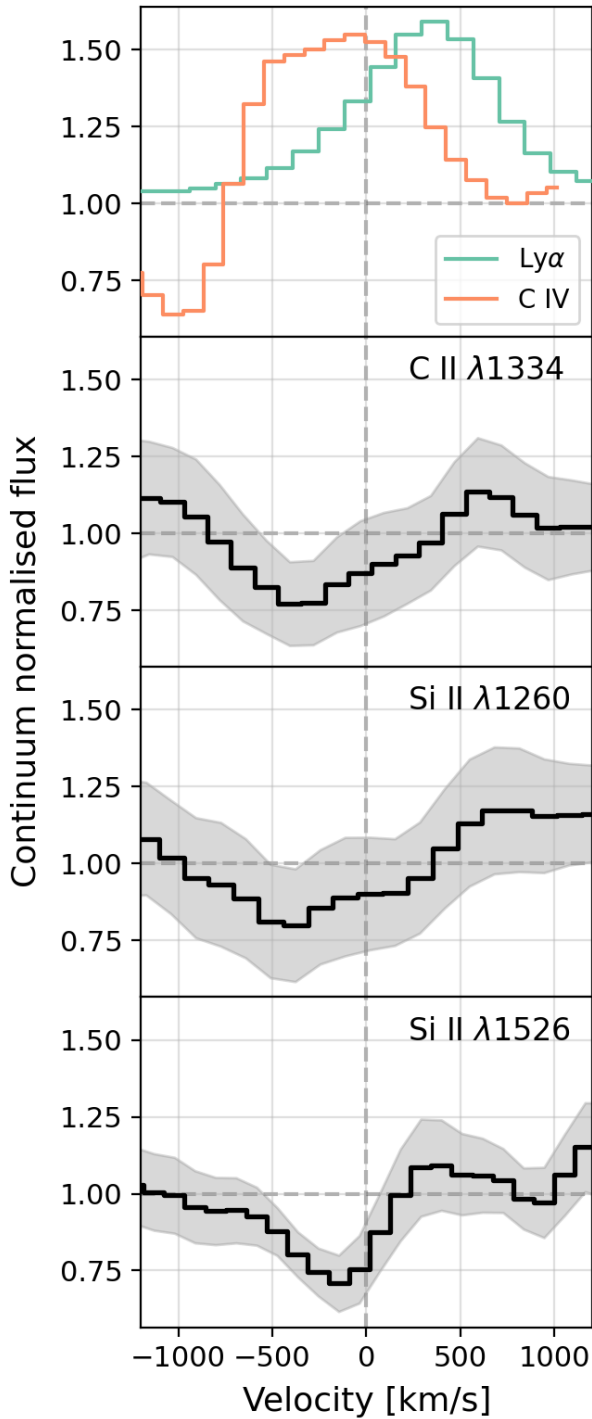


Figure 9. Low-ionisation interstellar (LIS) absorption of C II $\lambda 1334$, Si II $\lambda 1334$ and $\lambda 1526$ shown along with strong Ly α and C IV emission in the stacked spectrum. The shaded regions around the LIS lines are 1σ uncertainties calculated using bootstrapping. The systemic velocity $v = 0$ is set using C IV $\lambda 1550$. All features have been continuum normalised, with the Ly α line re-scaled for visualisation. The low covering fractions of LIS absorption features are indicative of relatively high f_{esc} (Mauerhofer et al. 2021; Saldana-Lopez et al. 2022), which also appear to be blue-shifted compared to the systemic velocity indicative of outflowing gas with velocities in the range $-500 \lesssim v \lesssim -200 \text{ km s}^{-1}$, consistent with measurements from known LyC leakers (e.g. Chisholm et al. 2017; Steidel et al. 2018).

one resolution element of the VANDELS spectra. The maximum covering fractions for the LIS gas are measured at $v \approx 150 - 400 \text{ km s}^{-1}$.

It is important to note that the scatter on the relation between f_{esc} and $\text{EW}_0(\text{LIS})$ can be large, and the relation is further sensitive to the spectral resolution as demonstrated by Saldana-Lopez et al. (2022). Those authors showed that these effects may increase the error on the inferred covering fractions by 5 – 20%, with a compounded effect on the uncertainty on f_{esc} . We further note that stacking the spectra of individual galaxies with varying outflow velocities may also muddle the absorption troughs by artificially broadening the absorption features, which has an important implication that f_{esc} measured from the covering fraction of LIS lines from stacked spectra will be an upper limit.

However, the widths of the LIS absorption features in the stacked spectrum appear to be fairly consistent with the spectral resolution of VANDELS, indicating that the individual outflow velocities do not vary dramatically across our sample. The outflow velocities for these lines that we infer are consistent with those measured for confirmed LyC leakers by Chisholm et al. (2017). We further note the remarkable resemblance of both the absorption profiles as well as the outflow velocities with the high f_{esc} sub-samples from Steidel et al. (2018), who also reported an increase in the depth of these absorption features with decreasing LyC f_{esc} .

5.4 C_{IV}/C_{III}] ratios for individual galaxies

In §2.2 we noted the presence of C_{III}] emission in 5 galaxies in our sample, and fortunately all 5 of these sources are likely to be star-forming galaxies (and not AGN). Schaerer et al. (2022) recently reported the detection of both C_{IV} and C_{III}] from a sample of confirmed LyC leaking galaxies at $z < 0.7$, and found strong LyC leakers ($f_{\text{esc}} > 0.1$) to have C_{IV}/C_{III}] ratios in excess of 0.75. Therefore, in this section we explore whether strong LyC leakage can be inferred, at least qualitatively, from galaxies in our sample with both C_{IV} and C_{III}] line detections.

Before comparing with measurements from low- z leakers, we note that in the analysis of Schaerer et al. (2022) the C_{IV} emission was likely purely nebular in origin, owing to a lack of P-Cygni absorption feature that is indicative of a stellar origin because of stellar photospheric absorption. We do note the presence of some absorption blueward of the C_{IV} line both in individual sources and the stacked spectrum, and we now attempt to capture the fraction of C_{IV} flux that could be attributed to stellar emission. To do this, we fit our individual galaxy spectra using SEDs that only contain stellar emission, taken from Saldana-Lopez et al. (2022). In short, these SEDs use STARBURST99 single star models (Leitherer et al. 2011) that include stellar rotation across a range of ages and metallicities. From this exercise, we find that on average $\approx 25\%$ of the C_{IV} flux may be attributed to stellar origin across our sample.

When plotting the C_{IV}/C_{III}] ratio in Figure 10, we have removed the stellar contribution to C_{IV} and only show the ratio of the nebular component of these lines as a function of $\text{EW}_0(\text{C}_4\text{V})$. We also show measurements from strong LyC leakers from Schaerer et al. (2022). Interestingly, based on this simple diagnostic we infer that 3 out of 5 galaxies in our sample that show both these lines lie in the regime of strong LyC leakage. We do note that the strength of C_{IV} emission from galaxies in our sample is systematically lower than what Schaerer et al. (2022) find for their LyC leakers.

Unfortunately, the C_{III}] line does not fall within the observed wavelength range of all galaxies in our final sample, and lying in a relatively redder part of the wavelength range of the spectrograph, the C_{III}] line is often contaminated by skyline residuals. Therefore,

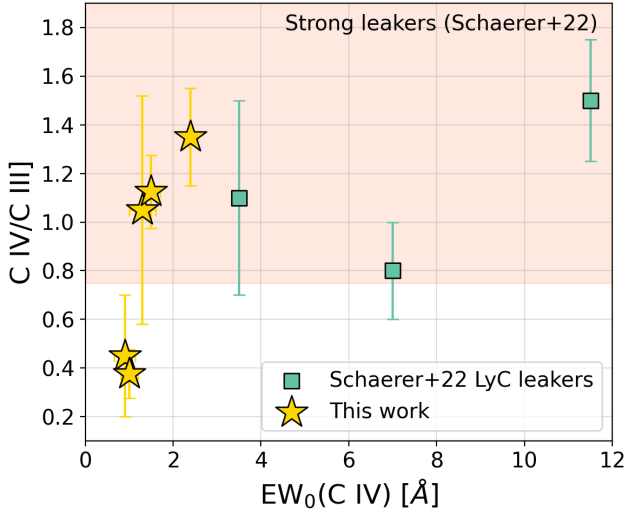


Figure 10. Ratio of nebular C IV and C III] versus $EW_0(C\text{ IV})$ for individual galaxies in this study where both lines are reliably detected. Also shown for comparison are measurements for confirmed LyC leaking galaxies at $z < 0.7$ from Schaerer et al. (2022). The shaded area represents the parameter space where Schaerer et al. (2022) found LyC leaking galaxies in their sample to lie. We find that 3 out of 5 galaxies in our sample that have both C IV and C III] detections show comparable C IV/C III] ratios to that of LyC leakers from Schaerer et al. (2022). We note that the $EW_0(C\text{ IV})$ for our galaxies are lower than that of low redshift leakers.

we choose not to consider C III] emission measures drawn from our stacked spectrum. However, from a very simple C IV/C III] ratio based diagnostic it is clear that strong LyC leakage may be expected from a fraction of C IV emitting galaxies in our sample, especially when considered in combination with other spectroscopic indicators in the stacked spectrum.

5.5 Concluding remarks on LyC escape

We conclude this section by reiterating the numerous lines of evidence supporting the contention that galaxies selected by their strong C IV emission have ISM conditions favourable for the escape of ionising LyC photons. These include strong Ly α emission line peaking close to the systemic redshift with non-zero flux bluewards of the peak, the presence of high-ionisation lines such as He II and low covering fractions of LIS absorption lines and their blue-shifted absorption troughs. We also find elevated C IV/C III] ratios observed in individual C IV emitters where both lines are robustly detected, which is also expected under conditions of significant LyC leakage.

The remarkable presence of all of these features together strongly indicates, albeit indirectly, that C IV emitting star-forming galaxies may be good candidates of strongly LyC leaking galaxies. With NIRSpec on board *JWST* it will be possible to detect C IV, He II and C III] emission from galaxies at $z > 6$, while probing absorption features from metals as well as neutral hydrogen gas in galaxies at even higher redshifts, possibly providing reliable observables to infer LyC f_{esc} in the epoch of reionisation. We have shown that galaxies exhibiting strong C IV have both high ξ_{ion} as well as potentially high f_{esc} , the product of which is a key ingredient to understand the role of star-forming galaxies towards the cosmic reionisation budget at $z > 6$.

6 SUMMARY

In this work we have identified 19 C IV emitting star-forming galaxies from the VANDELS survey spanning a redshift range $z = 3.1 - 4.6$ and presented their stacked spectrum (§2 and §3). Some individual C IV emitters show other rest-frame UV lines such as He II and O III] along with Ly α , and all of these lines are securely detected in the stacked spectrum allowing for a detailed analysis of the average properties of the underlying stellar populations as well as the interstellar medium in C IV emitting galaxies.

We show that the inferred rest-frame UV line fluxes and ratios from the stacked spectrum of C IV emitting galaxies at $z \sim 3.6$ suggest that they are comparable in ionisation properties to local C IV (and He II) emitting metal-poor galaxies, that have long been touted as analogues of reionisation era galaxies. We also find that the line strengths in the stack are similar to a handful of known C IV emitting sources at $z > 6$ (§3.3).

For the stacked spectrum of C IV emitters, we find that the best-fit spectral energy distribution (SED) models incorporating both stellar continuum and nebular line emission have low stellar metallicities of $Z = 0.1 - 0.2Z_{\odot}$, a young stellar ages of $\log(\text{age}/\text{yr}) = 6.1 - 6.5$, a high ionisation parameter $\log(U) = -2.0$ and little to no dust ($E(B - V) = 0.00 - 0.01$). This suggests that the presence of young, metal-poor stellar populations is necessary to explain the strong C IV (and other rest-UV) line emission seen across our sample (§4.1).

We also measure the average stellar metallicity of C IV emitters from the stacked spectrum using absorption indices at 1501 Å and 1719 Å that are sensitive to the metal content of stars. Both indices give a stellar metallicity of $Z \approx 0.2Z_{\odot}$ within errors, which is consistent with the the metallicity of SED model with $\log(\text{age}/\text{yr}) = 6.1$ and a small dust attenuation of $E(B - V) = 0.01$ (§4.2).

However, we find that the SED with $Z \approx 0.2Z_{\odot}$ under-predicts the C IV equivalent width by a factor of 3, and the He II equivalent width by a factor of 10. Since extremely young/metal-poor stars are needed to increase the predicted C IV and He II line fluxes from models, the observations of these strong lines and relatively higher metallicities suggest that a relatively young starburst event within a galaxy containing older populations may be able to explain the observed spectral features of our stacked spectrum (§4.3).

We then investigate whether galaxies showing strong C IV emission may exhibit significant hydrogen ionising LyC photon leakage into the intergalactic medium using a variety of indicators (§5). First, we find that the strength and shape of the Ly α emission in the stack is indicative of significant LyC leakage, as the Ly α line peaks close to the systemic velocity and contains non-zero flux blueward of the peak (§5.1). The presence of strong He II emission is indicative of substantial production of high-energy photons from young stars, and is consistent with what has been observed in the spectra of known LyC leaking galaxies (§5.2). The low equivalent widths and outflow velocities of low-ionisation interstellar absorption features are indicative of low column density channels through which LyC photons may escape, with their low covering fractions suggesting LyC $f_{\text{esc}} \approx 0.05 - 0.30$ (§5.3). Finally, the C IV/C III] ratio of a fraction of C IV emitting galaxies is comparable to measurements from other known LyC leakers in the low redshift Universe (§5.4).

We therefore conclude that C IV emitting galaxies harbour young stellar populations, tracing recent starburst events that leads to the production of copious amounts of ionising photons. This starburst phase is needed to displace neutral as well as low-ionisation gas in the ISM of galaxies, potentially creating holes in the ISM through which LyC photons may be able to escape into the IGM. We find indirect evidence of significant LyC leakage from C IV emitting galaxies,

suggesting that such galaxies could be important contributors towards cosmic reionisation at $z > 6$. Conditions leading to strong CIV emission may be ubiquitous across galaxies at very high redshifts when the stellar populations were young and star-formation from metal-deficient gas was widespread.

At $z \gtrsim 6$ when the increased neutrality of the IGM attenuates Ly α photons along the line-of-sight, the CIV line may offer a reliable alternative to identify galaxies with significant f_{esc} , which will be possible for statistical samples using *JWST*/NIRSpec. However, careful radiative transfer modelling of CIV and LyC is needed to theoretically back up any dependence of CIV and f_{esc} . Therefore, the presence of strong CIV emission combined with other rest-UV indicators in the spectra of galaxies at $z > 6$ can help establish whether they are likely contributors towards cosmic reionisation at early epochs.

ACKNOWLEDGEMENTS

AS thanks Silvia Genovese for assistance with plots and figures. AS and RSE acknowledge financial support from European Research Council Advanced Grant FP7/669253. ASL and DS acknowledge support from Swiss National Science Foundation.

This work makes use of VANDELS data. The VANDELS collaboration acknowledges the invaluable role played by ESO staff for successfully carrying out the survey.

This work has made extensive use of Jupyter and IPython (Pérez & Granger 2007) notebooks, Astropy (Astropy Collaboration et al. 2018), hoki (Stevance et al. 2020), matplotlib (Hunter 2007) and seaborn (Waskom & the seaborn development team 2020). This work would not have been possible without the countless hours put in by members of the open-source developing community all around the world.

DATA AVAILABILITY

The VANDELS Data Release 4 (DR4) is now publicly available and can be accessed using the VANDELS database at <http://vandels.inaf.it/dr4.html>, or through the ESO archives. The data analysis code was written in PYTHON and may be shared upon reasonable written request to the corresponding author.

REFERENCES

Astropy Collaboration et al., 2018, *AJ*, **156**, 123
 Barrow K. S. S., Robertson B. E., Ellis R. S., Nakajima K., Saxena A., Stark D. P., Tang M., 2020, *ApJ*, **902**, L39
 Berg D. A., Skillman E. D., Henry R. B. C., Erb D. K., Carigi L., 2016, *ApJ*, **827**, 126
 Berg D. A., Erb D. K., Auger M. W., Pettini M., Brammer G. B., 2018, *ApJ*, **859**, 164
 Berg D. A., Chisholm J., Erb D. K., Pogge R., Henry A., Olivier G. M., 2019, *ApJ*, **878**, L3
 Berg D. A., et al., 2022, arXiv e-prints, p. arXiv:2203.07357
 Bouwens R. J., Illingworth G. D., Oesch P. A., Caruana J., Holwerda B., Smit R., Wilkins S., 2015, *ApJ*, **811**, 140
 Calabro A., et al., 2021, *A&A*, **646**, A39
 Chisholm J., Orlitová I., Schaefer D., Verhamme A., Worseck G., Izotov Y. I., Thuan T. X., Guseva N. G., 2017, *A&A*, **605**, A67
 Chisholm J., et al., 2018, *A&A*, **616**, A30
 Cullen F., et al., 2020, *MNRAS*, **495**, 1501
 Dayal P., Ferrara A., 2018, *Phys. Rep.*, **780**, 1
 Dijkstra M., 2014, *Publ. Astron. Soc. Australia*, **31**, e040
 Dijkstra M., Gronke M., Venkatesan A., 2016, *ApJ*, **828**, 71
 Erb D. K., et al., 2014, *ApJ*, **795**, 33
 Feltre A., Charlot S., Gutkin J., 2016, *MNRAS*, **456**, 3354
 Feltre A., et al., 2020, *A&A*, **641**, A118
 Ferland G. J., et al., 2013, *Rev. Mex. Astron. Astrofis.*, **49**, 137
 Finkelstein S. L., et al., 2015, *ApJ*, **810**, 71
 Fletcher T. J., Tang M., Robertson B. E., Nakajima K., Ellis R. S., Stark D. P., Inoue A., 2019, *ApJ*, **878**, 87
 Flury S. R., et al., 2022a, arXiv e-prints, p. arXiv:2201.11716
 Flury S. R., et al., 2022b, arXiv e-prints, p. arXiv:2203.15649
 Garilli B., et al., 2021, *A&A*, **647**, A150
 Gazagnes S., Chisholm J., Schaefer D., Verhamme A., Izotov Y., 2020, *A&A*, **639**, A85
 Götberg Y., de Mink S. E., Groh J. H., Leitherer C., Norman C., 2019, *A&A*, **629**, A134
 Grazian A., et al., 2016, *A&A*, **585**, A48
 Guaita L., et al., 2016, *A&A*, **587**, A133
 Gutkin J., Charlot S., Bruzual G., 2016, *MNRAS*, **462**, 1757
 Henry A., Scarlata C., Martin C. L., Erb D., 2015, *ApJ*, **809**, 19
 Hunter J. D., 2007, *Computing In Science & Engineering*, **9**, 90
 Inoue A. K., Shimizu I., Iwata I., Tanaka M., 2014, *MNRAS*, **442**, 1805
 Izotov Y. I., Schaefer D., Worseck G., Guseva N. G., Thuan T. X., Verhamme A., Orlitová I., Fricke K. J., 2018, *MNRAS*, **474**, 4514
 Izotov Y. I., Worseck G., Schaefer D., Guseva N. G., Chisholm J., Thuan T. X., Fricke K. J., Verhamme A., 2021, *MNRAS*, **503**, 1734
 Jones T., Stark D. P., Ellis R. S., 2012, *ApJ*, **751**, 51
 Jones T. A., Ellis R. S., Schenker M. A., Stark D. P., 2013, *ApJ*, **779**, 52
 Katz H., et al., 2020, *MNRAS*, **498**, 164
 Kimm T., Bieri R., Geen S., Rosdahl J., Blaizot J., Michel-Dansac L., Garel T., 2022, *ApJS*, **259**, 21
 Kocevski D. D., et al., 2018, *ApJS*, **236**, 48
 Laporte N., Meyer R. A., Ellis R. S., Robertson B. E., Chisholm J., Roberts-Borsani G. W., 2021, *MNRAS*, **505**, 3336
 Le Fèvre O., et al., 2019, *A&A*, **625**, A51
 Leethochawalit N., Jones T. A., Ellis R. S., Stark D. P., Zitrin A., 2016, *ApJ*, **831**, 152
 Leitherer C., et al., 2011, Starburst99: Synthesis Models for Galaxies with Active Star Formation, Astrophysics Source Code Library, record ascl:1104.003 (ascl:1104.003)
 Llerena M., et al., 2021, arXiv e-prints, p. arXiv:2107.00660
 Luo B., et al., 2017, *ApJS*, **228**, 2
 Mainali R., Kollmeier J. A., Stark D. P., Simcoe R. A., Walth G., Newman A. B., Miller D. R., 2017, *ApJ*, **836**, L14
 Marchi F., et al., 2017, *A&A*, **601**, A73
 Marques-Chaves R., et al., 2022, arXiv e-prints, p. arXiv:2205.05567
 Matthee J., et al., 2022, *A&A*, **660**, A10
 Mauerhofer V., Verhamme A., Blaizot J., Garel T., Kimm T., Michel-Dansac L., Rosdahl J., 2021, *A&A*, **646**, A80
 McLure R. J., et al., 2018, *MNRAS*, **479**, 25
 Meštrić U., Ryan-Weber E. V., Cooke J., Bassett R., Prichard L. J., Rafelski M., 2021, *MNRAS*, **508**, 4443
 Naidu R. P., Forrest B., Oesch P. A., Tran K.-V. H., Holden B. P., 2018, *MNRAS*, **478**, 791
 Naidu R. P., et al., 2022, *MNRAS*, **510**, 4582
 Nakajima K., Ouchi M., 2014, *MNRAS*, **442**, 900
 Nakajima K., Fletcher T., Ellis R. S., Robertson B. E., Iwata I., 2018b, *MNRAS*, **477**, 2098
 Nakajima K., Fletcher T., Ellis R. S., Robertson B. E., Iwata I., 2018a, *MNRAS*, **477**, 2098
 Nakajima K., Ellis R. S., Robertson B. E., Tang M., Stark D. P., 2020, *ApJ*, **889**, 161
 Nanayakkara T., et al., 2019, *A&A*, **624**, A89
 Pentericci L., et al., 2018, *A&A*, **616**, A174
 Pérez F., Granger B. E., 2007, *Computing in Science and Engineering*, **9**, 21
 Planck Collaboration et al., 2016, *A&A*, **594**, A13
 Plat A., Charlot S., Bruzual G., Feltre A., Vidal-García A., Morisset C., Chevallard J., Todt H., 2019, *MNRAS*, **490**, 978

Reddy N. A., Steidel C. C., Pettini M., Bogosavljević M., 2016a, *ApJ*, **828**, 107

Reddy N. A., Steidel C. C., Pettini M., Bogosavljević M., Shapley A. E., 2016b, *ApJ*, **828**, 108

Reddy N. A., et al., 2022, *ApJ*, **926**, 31

Rivera-Thorsen T. E., et al., 2019, *Science*, **366**, 738

Roberts-Borsani G. W., Ellis R. S., Laporte N., 2020, *MNRAS*, **497**, 3440

Robertson B. E., et al., 2013, *ApJ*, **768**, 71

Robertson B. E., Ellis R. S., Furlanetto S. R., Dunlop J. S., 2015, *ApJ*, **802**, L19

Saldana-Lopez A., et al., 2022, arXiv e-prints, p. [arXiv:2201.11800](https://arxiv.org/abs/2201.11800)

Saxena A., et al., 2020a, *MNRAS*, **496**, 3796

Saxena A., et al., 2020b, *A&A*, **636**, A47

Saxena A., et al., 2022, *MNRAS*, **511**, 120

Schaerer D., Fragos T., Izotov Y. I., 2019, *A&A*, **622**, L10

Schaerer D., et al., 2022, *A&A*, **658**, L11

Schmidt K. B., et al., 2017, *ApJ*, **839**, 17

Senchyna P., et al., 2017, *MNRAS*, **472**, 2608

Senchyna P., Stark D. P., Chevallard J., Charlot S., Jones T., Vidal-García A., 2019, *MNRAS*, **488**, 3492

Senchyna P., Stark D. P., Charlot S., Chevallard J., Bruzual G., Vidal-García A., 2021, *MNRAS*, **503**, 6112

Shapley A. E., Steidel C. C., Pettini M., Adelberger K. L., Erb D. K., 2006, *ApJ*, **651**, 688

Shivaei I., et al., 2018, *ApJ*, **855**, 42

Simmonds C., Schaerer D., Verhamme A., 2021, *A&A*, **656**, A127

Stanway E. R., Eldridge J. J., 2018, *MNRAS*, **479**, 75

Stanway E. R., Eldridge J. J., Becker G. D., 2016, *MNRAS*, **456**, 485

Stark D. P., et al., 2015, *MNRAS*, **454**, 1393

Steidel C. C., Strom A. L., Pettini M., Rudie G. C., Reddy N. A., Trainor R. F., 2016, *ApJ*, **826**, 159

Steidel C. C., Bogosavljević M., Shapley A. E., Reddy N. A., Rudie G. C., Pettini M., Trainor R. F., Strom A. L., 2018, *ApJ*, **869**, 123

Stevance H., Eldridge J., Stanway E., 2020, *The Journal of Open Source Software*, **5**, 1987

Tang M., Stark D. P., Chevallard J., Charlot S., Endsley R., Congiu E., 2021, *MNRAS*, **501**, 3238

Tang M., Stark D. P., Ellis R. S., 2022, arXiv e-prints, p. [arXiv:2202.04142](https://arxiv.org/abs/2202.04142)

Umeda H., Ouchi M., Nakajima K., Isobe Y., Aoyama S., Harikane Y., Ono Y., Matsumoto A., 2022, arXiv e-prints, p. [arXiv:2201.06593](https://arxiv.org/abs/2201.06593)

Vanzella E., et al., 2016, *ApJ*, **821**, L27

Vanzella E., et al., 2018, *MNRAS*, **476**, L15

Vanzella E., et al., 2021, *A&A*, **646**, A57

Verhamme A., Orlitová I., Schaerer D., Hayes M., 2015, *A&A*, **578**, A7

Verhamme A., Orlitová I., Schaerer D., Izotov Y., Worseck G., Thuan T. X., Guseva N., 2017, *A&A*, **597**, A13

Waskom M., the seaborn development team 2020, mwaskom/seaborn, doi:10.5281/zenodo.592845, <https://doi.org/10.5281/zenodo.592845>

Witstok J., Smit R., Maiolino R., Curti M., Laporte N., Massey R., Richard J., Swinbank M., 2021, *MNRAS*, **508**, 1686

Xiao L., Stanway E. R., Eldridge J. J., 2018, *MNRAS*, **477**, 904

This paper has been typeset from a $\text{\TeX}/\text{\LaTeX}$ file prepared by the author.